Engineering antiphase boundaries in epitaxial SrTiO₃ to achieve forming free memristive devices

Felix V. E. Hensling ⓘD, Hongchu Du ⓘD, Nicolas Raab, Chun-Lin Jia, Joachim Mayer, and Regina Dittmann ⓘD

View Online   Export Citation   CrossMark

ARTICLES YOU MAY BE INTERESTED IN

APL Materials

AIP Publishing

Engineering antiphase boundaries in epitaxial SrTiO₃ to achieve forming free memristive devices

View Online   Export Citation   CrossMark

Felix V. E. Hensling,[1,2,a)] iD Hongchu Du,[2,3,4] iD Nicolas Raab,[1,2] Chun-Lin Jia,[5,6] Joachim Mayer,[2,3,4] and Regina Dittmann[1,2] iD

AFFILIATIONS

[1] PGI-7, Forschungszentrum Jülich GmbH, 52425 Jülich, Germany
[2] JARA-FIT, Forschungszentrum Jülich GmbH, 52425 Jülich, Germany
[3] ER-C 2, Forschungszentrum Jülich GmbH, 52425 Jülich, Germany
[4] GFE, RWTH Aachen University, 52074 Aachen, Germany
[5] ER-C 1, Forschungszentrum Jülich GmbH, 52425 Jülich, Germany
[6] PGI-5, Forschungszentrum Jülich GmbH, 52425 Jülich, Germany

[a)] Electronic mail: f.hensling@fz-juelich.de

ABSTRACT

We here present a method to engineer Ruddlesden-Popper-type antiphase boundaries in stoichiometric homoepitaxial SrTiO₃ thin films. This is achieved by using a substrate with an intentionally high miscut, which stabilizes the growth of additional SrO at the bottom interface. We prove the success of this strategy utilizing transmission electron microscopy. We find that these antiphase boundaries significantly influence the resistive switching properties. In particular, devices based on SrTiO₃ thin films with intentionally induced antiphase boundaries do not require a forming step, which is ascribed to the existence of preformed filaments.

Transition metal oxide materials have been the center of a wide range of research for decades as they are equipped with various interesting properties often connected to their outer d-electrons. These properties include, but are not limited to, their electronic and magnetic state.[1] Interestingly, these properties are often manifested by the oxide's defect structure as, for example, oxygen vacancy induced conduction.[2–5]

Another defect type with a central influence on the property of oxide thin films is antiphase boundaries. Known influences reach from the magnetic properties of the material[6,7] to its (super)conductivity[7–9] and its optical band gap.[10,11] It is therefore not surprising that antiphase boundaries have been reported to significantly influence the performance for applications such as sensors,[12,13] thermoelectrics,[14] and resistive switching.[15,16] Thus, a controlled engineering of these antiphase boundaries is highly desirable and different strategies to achieve this have been investigated in the past. The two most prominent strategies are the introduction of antiphase boundaries by the lattice mismatch[17,18] or by

off-stoichiometry.[19–21] Both of these strategies, however, have certain drawbacks. For both strategies, the formation of antiphase boundaries throughout the thin film is random; utilizing the lattice mismatch further limits the choice of substrate materials, while an off-stoichiometric growth is usually accompanied by a wide variety of different defects besides antiphase boundaries. Recently, efforts have been made to achieve a more controllable formation of antiphase boundaries by choosing a substrate and thin film combination with nonsequential layers.[22]

A special type of antiphase boundary is the Ruddlesden-Popper-type antiphase boundary, which is typical for perovskites, in particular with Sr on the A-site.[23–25] For such perovskites, SrTiO₃ (STO) constitutes a model material, due to its well known defect chemistry. For STO, a Ruddlesden-Popper-type antiphase boundary can be described by a stacking fault of subsequent n SrO layers instead of alternating TiO₂ and SrO layers.

It has been shown that Sr-rich thin films exhibit Ruddlesden-Popper-type antiphase boundaries.[19,20] However, the growth of

Sr-rich thin films is accompanied by additional defects, such as Ti–O-vacancy clusters, which have drastic influences on the properties as well.[26–28] Furthermore, the formation of additional SrO layers within the thin film is often avoided by the additional SrO accumulating at the thin film's surface.[19,29] The challenge is, thus, to identify the correlation between changed properties of the thin film and the actual Ruddlesden-Popper-type antiphase boundaries.

In this paper, we present a technique to engineer Ruddlesden-Popper-type antiphase boundaries in otherwise stoichiometric epitaxial STO thin films. We are thus able to probe the influence of the said Ruddlesden-Popper-type antiphase boundaries independent from any other defect type. We apply this knowledge to demonstrate their effect on memristive devices based on STO thin films.

Resistive switching of memristive devices is based on the reversible change in the oxygen vacancy concentration induced during electrical biasing, which modulates the resistance between two states, the low resistive state (ON) and the high resistive state (OFF).[30–32] Usually, memristive devices require a forming step distinguishable by the increased voltage required for the first SET, which is highly undesirable for an application in complex circuits.[33]

We here present that the intentionally induced Ruddlesden-Popper-type antiphase boundaries can be utilized to achieve forming free devices.

As substrates, 0.5 wt. %Nb:STO (100) are used. They are TiO$_2$-terminated by etching in buffered HF.[34] Nb:STO substrates offer the advantage of functioning as the bottom electrode and simultaneously enabling epitaxial growth. On these substrates, 1.5 u.c. of SrO is deposited by pulsed laser deposition (PLD) at 800 °C substrate temperature, 10^{-7} mbar oxygen pressure with a laser fluence of 0.81 J/cm^2 ablating a SrO$_2$ target.[35] The 15 nm STO film is subsequently deposited without exposure to ambient in the same PLD chamber ablating from an STO single crystal target at 0.1 mbar oxygen pressure and 800 °C substrate temperature with a fluence of 1.02 J/cm^2. These parameters result in high quality epitaxial stoichiometric STO thin films.[36–39] We here achieve a Schottky-type interface by depositing 30 nm of Pt on top of the thin films via e-beam evaporation. The Pt is patterned into 10×10 μm^2 square top electrodes using photolithography and Ar ion beam etching. We contact these Pt
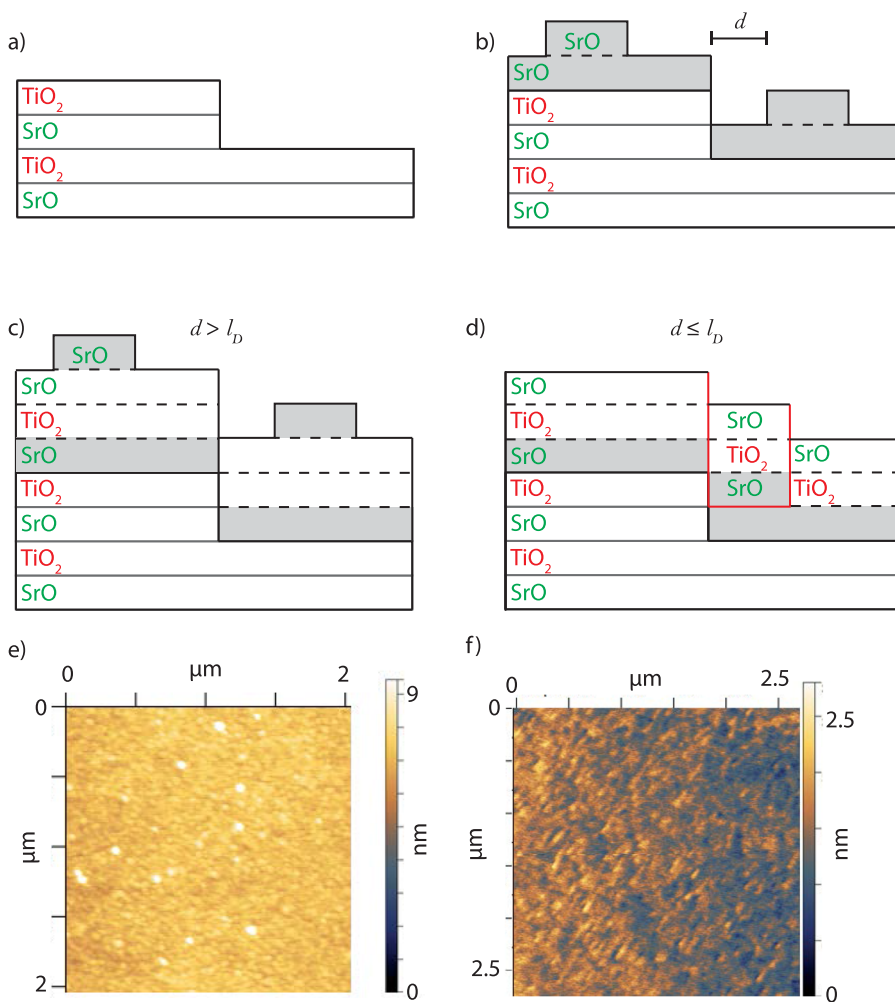
FIG. 1. [(a)–(d)] Schematics of stoichiometric STO grown at 800 °C on top of (a) a TiO$_2$-terminated Nb:STO substrate with (b) 1.5 u.c. of SrO deposited directly on the substrate. (c) Either the SrO migrates to the top and results in the topography of (e) or it is stabilized at the bottom interface (d) and induces antiphase boundaries (red lines), resulting in the topography (f).

electrodes with W-whisker probes, while the Nb:STO bottom electrode is grounded, to characterize the devices by using a *Keithley 2611A Source Meter*. Characterization is carried out applying a current compliance of 10 mA. The initial sweep is carried out at +3 V; as are all subsequent SETs, the RESET is carried out at −4 V.

Figure 1(a) shows the schematic of a TiO_2-terminated Nb:STO substrate with regular 1 u.c. steps. Depositing 1.5 u.c. of SrO on such a substrate first results in a change toward a SrO termination, which takes 1 u.c. The additional half u.c. would be expected to induce antiphase boundaries [Figs. 1(b) and 1(d)] due to the presence of half u.c. steps, similar to using a substrate and thin film combination with nonsequential layers.[22] However, the resulting topography in Fig. 1(e) reveals barely visible step edges and numerous islands. The surface is comparable to the one to be expected, when growing SrO islands on top of stoichiometric films.[35] It thus seems that the additional SrO did not remain at the bottom interface and induce antiphase boundaries as intended but rather ended up at the top interface. A behavior that has been observed previously[19,29] is schematically represented in Fig. 1(c).

The challenge is, thus, to prevent the additional SrO deposited at the bottom interface from migrating to the top interface. Generally, two strategies are conceivable for this. If the subsequent growth of STO is performed at a temperature low enough to suppress fast cation diffusion, a migration of the SrO layer to the surface is inhibited. This strategy inherently results in additional problems. A suppression of the cation diffusion results in thin films with additional extended defects and thus a poor crystal quality. The second strategy is to stabilize the SrO at step edges as species bond at step edges are energetically more stable. If the width of a step is comparably high, the distance d the additional SrO needs to overcome to stabilize at a step edge is on average longer than its diffusion-length l_D; it will thus not reach the step edge [Fig. 1(c)]. If the width of a step, however, is comparably narrow, the distance d the additional SrO needs to overcome to stabilize at a step edge is on average shorter than its diffusion-length l_D; it can thus stabilize at the step edge [Fig. 1(d)]. The single-layer SrO island stabilized at the step edge can be regarded as a spatially restricted horizontal antiphase boundary. At its edges, it induces vertical antiphase boundaries, as depicted in Fig. 1(d).

To utilize this, Nb:STO substrates with an intentionally high miscut and thus a high step density are selected. A miscut of 4° in the (010) direction is chosen. Figure 1(f) shows the topography of a stoichiometric STO film grown on top of 1.5 u.c. of SrO, which were grown on the 4° miscut TiO_2-terminated Nb:STO substrate. This results in a thin film, which shows no SrO segregation, as schematically shown in Fig. 1(d). Furthermore, the dense step edge structure remains observable. It is thus probable that the 1.5 u.c. of SrO is indeed located within the film. To verify this, scanning transmission electron microscopy (STEM) is performed.

Figure 2(a) shows a high-angle annular dark-field (HAADF) STEM survey of a step edge and the interface between a 4° miscut TiO_2-terminated Nb:STO substrate with 1.5 u.c. of SrO on top and a stoichiometric STO thin film. It reveals a high crystal quality, which is only disturbed by the intentionally induced antiphase boundaries. As intended, additional to the antiphase boundary at the interface between the substrate and STO film, induced by the additional SrO layer, an antiphase boundary was induced perpendicular at the step edge continuing throughout the film, as indicated

by the unit cell illustrations for orientation with Ti represented by red spheres and Sr by green. Figure 2(b) shows a close-up HAADF STEM of the antiphase boundary at the bottom interface. In Fig. 2(c), the cations are marked in red (Ti) and green (Sr) for better visibility. The false color map of the interface in Fig. 2(d) verifies the existence of the double layer of SrO. It further reveals a contrast increase in the first subsequent layer of TiO_2, which is even clearer in the averaged profile in Fig. 2(e). The atomic-resolution electron energy loss spectroscopy (EELS) map in Fig. 2(f) evidently reveals a $TiO_2/SrO/SrO/TiO_2$ stack as well. The increase of HAADF contrast
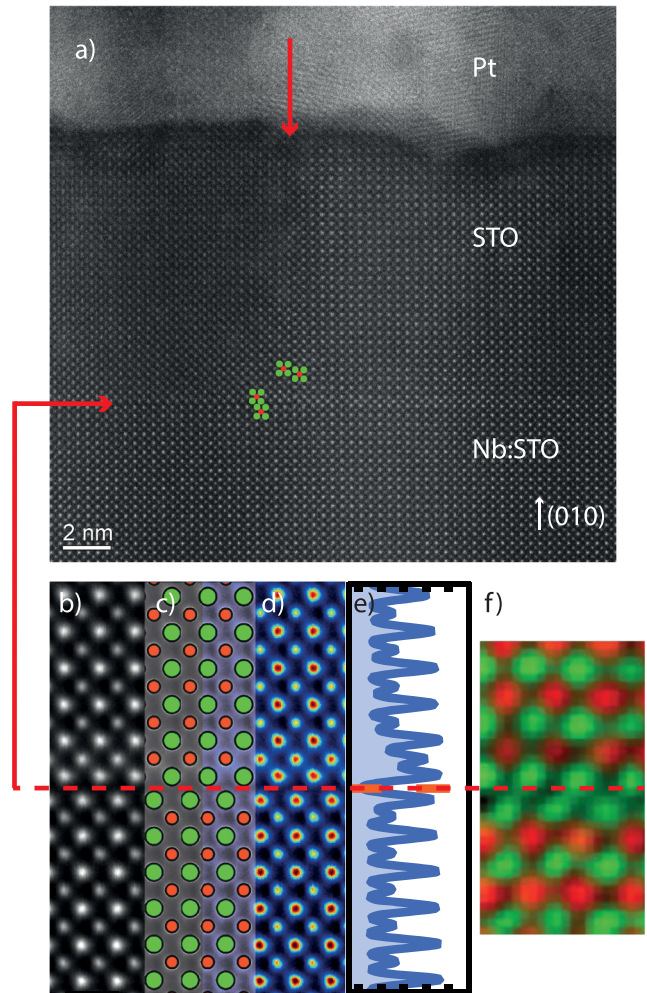
FIG. 2. (a) HAADF TEM survey of the stoichiometric STO thin film grown on 1.5 u.c. of SrO on top of TiO_2-terminated Nb:STO showing a vertical antiphase boundary induced at the step edge with a structural model for orientation. As the lattices along the horizontal direction is periodical, it is averaged to reduce the noise and scanning distortions. (b) Close-up of the antiphase boundary with (c) structural model of the interface with green representing Sr and red Ti. (d) False color map of the interface between the substrate and film obtained by HAADF clearly revealing a double layer of Sr. (e) Averaged profile, which clearly reveals the interface comprising an antiphase boundary. (f) Denoised EELS map of the antiphase boundary with Sr L represented in green and Ti L represented in red, confirming a $TiO_2/SrO/SrO/TiO_2$ stack.

for the first subsequent layer of TiO$_2$ may be associated with a very small amount of Sr randomly occupying at Ti sites and small lattice distortions or atomic displacements induced by such underlying defects.

Having successfully engineered Ruddlesden-Popper-type antiphase boundaries in otherwise stoichiometric thin films allows us to investigate their influence on resistive switching. Figure 3(a) shows the $I(V)$-characteristics of the first sweep (red) and a subsequent SET (blue) of a stoichiometric device as reference for Fig. 3(b), which shows the same for a device with intentionally induced antiphase boundaries. Considering the annular bright-field STEM overview in the supplementary material Fig. 1, we can expect an average of around 6 perpendicular antiphase boundaries per 100 nm. This would result in an estimate of 600 per device. Considering the stoichiometric device in Fig. 3(a), it is obvious that a higher voltage is needed to reach the current compliance and, thus, to change

from the virgin state 1 (red) into the LRS than for all subsequent SETs (blue). As a result, for each voltage, the current is higher for all subsequent SETs (blue) than for the first SET (red). The device thus requires a forming step. In terms of the application of resistive switching in complex circuits, a forming step is highly undesirable. The avoidance of such a forming step is, thus, of central interest in the field of resistive switching.[33,40] Comparing the $I(V)$-characteristics of the device with intentionally induced antiphase boundaries in Fig. 3(b), it is noticeable that no forming step is observable. The first sweep (red) is identical to the subsequent SETs (blue). The device is thus forming free.

A possible mechanism is illustrated next to the respective $I(V)$-characteristics in Fig. 3. Recent studies have revealed that resistive switching of STO in the considered configuration is based on the release and reincorporation of molecular oxygen. In particular, each SET is accompanied by the formation of molecular oxygen,
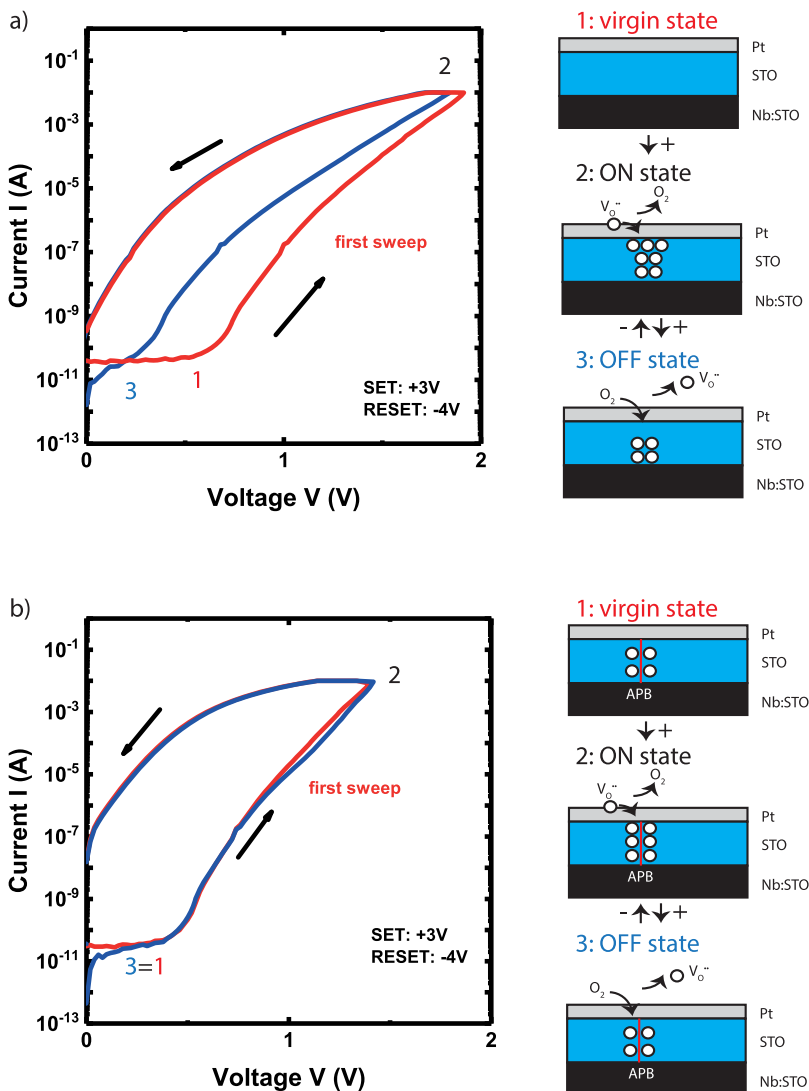
FIG. 3. (a) IV-characteristic of a stoichiometric device including an illustration of the filament formation mechanism and (b) IV-characteristic of a device with induced antiphase boundaries, not requiring a forming step (red) as a preformed filament forms along the antiphase boundary.

which is either stored in the Pt or released into air, resulting in the formation of oxygen vacancies (step 2 in Fig. 3). Each RESET is then achieved by the reincorporation of oxygen, from either air or the electrode material (step 3 in Fig. 3).[41,42] As the devices with intentionally induced Ruddlesden-Popper type antiphase boundaries are forming-free, an obvious explanation is the presence of a preformed filament in the virgin state. Furthermore, the only difference between these devices and normal stoichiometric devices is the Ruddlesden-Popper type antiphase boundaries, which are the only extended defects present due to the epitaxial nature of the thin films. It is thus likely that the Ruddlesden-Popper type antiphase boundaries are connected to the preformed filaments. A possible explanation is an enrichment in naturally occurring oxygen vacancies[43,44] at the Ruddlesden-Popper type antiphase boundaries. This is conceivable as it was reported for other extended defects in STO, namely, small angle grain boundaries[45,46] and dislocations.[46–48] For these defects, the formation energy of oxygen vacancies is lower in the defect's vicinity.[45–48] If the formation of oxygen vacancies is lower at Ruddlesden-Popper type antiphase boundaries, it is conceivable that this naturally occurring oxygen vacancy rich region is the preformed filament, ultimately explaining the lack of a forming step.

Summarizing, we have shown in this work how to successfully induce Ruddlesden-Popper type antiphase boundaries in otherwise stoichiometric STO thin films. This can be achieved by the deposition of 1.5 u.c. of SrO on an intentionally miscut TiO$_2$-terminated Nb:STO substrate. The additional SrO at the bottom interface induces horizontal and vertical Ruddlesden-Popper type antiphase boundaries. The resulting STO thin films can be used to achieve forming free memristive devices.

The principle shown here to induce Ruddlesden-Popper type antiphase boundaries in otherwise stoichiometric thin films should be applicable to all perovskites with the ability to form this type of antiphase boundary.

See supplementary material for an annular bright-field STEM overview to elucidate the density and periodicity of perpendicular antiphase boundaries.

REFERENCES

[1] C. Rao, Annu. Rev. Phys. Chem. **40**, 291 (1989).
[2] R. Moos, W. Menesklou, and K. H. Hardtl, Appl. Phys. A: Mater. Sci. Process. **61**, 389 (1995).
[3] R. Moos and K. H. Hardtl, J. Am. Ceram. Soc. **80**, 2549 (1997).
[4] F. Gunkel, S. Hoffmann-Eifert, R. Dittmann, S. B. Mi, C. L. Jia, P. Meuffels, and R. Waser, Appl. Phys. Lett. **97**, 012103 (2010).
[5] F. V. E. Hensling, C. Xu, F. Gunkel, and R. Dittmann, Sci. Rep. **7**, 39953 (2017).
[6] A. Bollero, M. Ziese, R. Höhne, H. C. Semmelhack, U. Köhler, A. Setzer, and P. Esquinazi, J. Magn. Magn. Mater. **285**, 279 (2005).
[7] J. B. Goodenough and R. I. Dass, Int. J. Inorg. Mater. **2**, 3 (2000).
[8] S. K. Arora, R. G. Sofin, I. V. Shvets, R. Kumar, M. W. Khan, and J. P. Srivastava, J. Appl. Phys. **97**, 10C310 (2005).
[9] G. Rijnders, S. Currás, M. Huijben, D. H. Blank, and H. Rogalla, Appl. Phys. Lett. **84**, 1150 (2004).
[10] A. H. Reshak, S. Auluck, and I. Kityk, Jpn. J. Appl. Phys., Part 1 **47**, 5516 (2008).
[11] C. H. Lee, N. J. Podraza, Y. Zhu, R. F. Berger, S. Shen, M. Sestak, R. W. Collins, L. F. Kourkoutis, J. A. Mundy, H. Wang, Q. Mao, X. Xi, L. J. Brillson, J. B. Neaton, D. A. Muller, and D. G. Schlom, Appl. Phys. Lett. **102**, 122901 (2013).
[12] W. Menesklou, H. J. Schreiner, K. H. Härdtl, and E. Ivers-Tiffée, Sens. Actuators, B **59**, 184 (1999).
[13] T. Hara, T. Ishiguro, and K. Shinozaki, Jpn. J. Appl. Phys., Part 2 **49**, 09MA15 (2010).
[14] C. M. Brooks, R. B. Wilson, A. Schäfer, J. A. Mundy, M. E. Holtz, D. A. Muller, J. Schubert, D. G. Cahill, and D. G. Schlom, Appl. Phys. Lett. **107**, 051902 (2015).
[15] K. Shibuya, R. Dittmann, S. Mi, and R. Waser, Adv. Mater. **22**, 411 (2010).
[16] N. Raab, C. Bäumer, and R. Dittmann, AIP Adv. **5**, 047150 (2015).
[17] M. Luysberg, R. G. Sofin, S. K. Arora, and I. V. Shvets, Phys. Rev. B **80**, 024111 (2009).
[18] I. MacLaren, B. Sala, S. M. Andersson, T. J. Pennycook, J. Xiong, Q. X. Jia, E. M. Choi, and J. L. MacManus-Driscoll, Nanoscale Res. Lett. **10**, 407 (2015).
[19] C. Xu, H. Du, A. J. Van Der Torren, J. Aarts, C. L. Jia, and R. Dittmann, Sci. Rep. **6**, 38296 (2016).
[20] Y. Tokuda, S. Kobayashi, T. Ohnishi, T. Mizoguchi, N. Shibata, Y. Ikuhara, and T. Yamamoto, Appl. Phys. Lett. **99**, 033110 (2011).
[21] C. M. Brooks, L. F. Kourkoutis, T. Heeg, J. Schubert, D. A. Muller, and D. G. Schlom, Appl. Phys. Lett. **94**, 162905 (2009).
[22] Z. Wang, H. Guo, S. Shao, M. Saghayezhian, J. Li, R. Fittipaldi, A. Vecchione, P. Siwakoti, Y. Zhu, J. Zhang, and E. W. Plummer, Proc. Natl. Acad. Sci. U. S. A. **115**, 9485 (2018).
[23] J. H. Lee, G. Luo, I. C. Tung, S. H. Chang, Z. Luo, M. Malshe, M. Gadre, A. Bhattacharya, S. M. Nakhmanson, J. A. Eastman, H. Hong, J. Jellinek, D. Morgan, D. D. Fong, and J. W. Freeland, Nat. Mater. **13**, 879 (2014).
[24] J. H. Haeni, C. D. Theis, D. G. Schlom, W. Tian, X. Q. Pan, H. Chang, I. Takeuchi, and X. D. Xiang, Appl. Phys. Lett. **78**, 3292 (2001).
[25] J. S. Wu, C. L. Jia, K. Urban, J. H. Hao, and X. X. Xi, J. Cryst. Growth **234**, 603 (2002).
[26] T. Ohnishi, M. Lippmaa, T. Yamamoto, S. Meguro, and H. Koinuma, Appl. Phys. Lett. **87**, 241919 (2005).
[27] E. Breckenfeld, R. Wilson, J. Karthik, A. R. Damodaran, D. G. Cahill, and L. W. Martin, Chem. Mater. **24**, 331 (2012).
[28] D. J. Keeble, S. Wicklein, L. Jin, C. L. Jia, W. Egger, and R. Dittmann, Phys. Rev. B **87**, 195409 (2013).
[29] Y. F. Nie, Y. Zhu, C.-H. Lee, L. F. Kourkoutis, J. A. Mundy, J. Junquera, P. Ghosez, D. J. Baek, S. Sung, X. X. Xi, K. M. Shen, D. A. Muller, and D. G. Schlom, Nat. Commun. **5**, 4530 (2014).
[30] R. Waser, R. Dittmann, M. Salinga, and M. Wuttig, Solid-State Electron. **54**, 830 (2010).
[31] K. Szot, R. Dittmann, W. Speier, and R. Waser, Phys. Status Solidi RRL **1**, R86 (2007).
[32] K. Szot, W. Speier, G. Bihlmayer, and R. Waser, Nat. Mater. **5**, 312 (2006).
[33] R. S. Williams, Faraday Discuss. **213**, 579 (2019).
[34] M. Kawasaki, K. Takahashi, T. Maeda, R. Tsuchiya, M. Shinohara, O. Ishiyama, T. Yonezawa, M. Yoshimoto, and H. Koinuma, Science **266**, 1540 (1994).
[35] F. Hensling, T. Heisig, N. Raab, C. Baeumer, and R. Dittmann, Solid State Ionics **325**, 247 (2018).
[36] C. Xu, S. Wicklein, A. Sambri, S. Amoruso, M. Moors, and R. Dittmann, J. Phys. D: Appl. Phys. **47**, 034009 (2014).
[37] C. Xu, M. Moors, and R. Dittmann, Appl. Surf. Sci. **359**, 68 (2015).
[38] S. Wicklein, A. Sambri, S. Amoruso, X. Wang, R. Bruzzese, A. Koehl, and R. Dittmann, Appl. Phys. Lett. **101**, 131601 (2012).
[39] C. Baeumer, C. Xu, F. Gunkel, N. Raab, R. A. Heinen, A. Koehl, and R. Dittmann, Sci. Rep. **5**, 11829 (2015).
[40] S. Cho, C. Yun, S. Tappertzhofen, A. Kursumovic, S. Lee, P. Lu, Q. Jia, M. Fan, J. Jian, H. Wang, S. Hofmann, and J. L. MacManus-Driscoll, Nat. Commun. **7**, 12373 (2016).
[41] T. Heisig, C. Baeumer, U. N. Gries, M. P. Mueller, C. La Torre, M. Luebben, N. Raab, H. Du, S. Menzel, D. N. Mueller, C.-l. Jia, J. Mayer, R. Waser, I. Valov, R. A. De Souza, and R. Dittmann, Adv. Mater. **30**, 1800957 (2018).

[42] D. Cooper, C. Baeumer, N. Bernier, A. Marchewka, C. La Torre, R. E. Dunin-Borkowski, S. Menzel, R. Waser, and R. Dittmann, Adv. Mater. **29**, 1700212 (2017).

[43] F. Oba, M. Choi, A. Togo, A. Seko, and I. Tanaka, J. Phys.: Condens. Matter **22**, 384211 (2010).

[44] M. M. Rutkowski, K. McNicholas, Z. Q. Zeng, F. Tuomisto, and L. J. Brillson, J. Phys. D: Appl. Phys. **47**, 255303 (2014).

[45] Z. Zhang, W. Sigle, R. A. De Souza, W. Kurtz, J. Maier, and M. Rühle, Acta Mater. **53**, 5007 (2005).

[46] R. A. Souza, J. Fleig, J. Maier, O. Kienzle, Z. Zhang, W. Sigle, and M. Rühle, J. Am. Ceram. Soc. **86**, 922 (2003).

[47] D. Marrocchelli, L. Sun, and B. Yildiz, J. Am. Chem. Soc. **137**, 4735 (2015).

[48] R. A. De Souza, V. Metlenko, D. Park, and T. E. Weirich, Phys. Rev. B **85**, 174109 (2012).